15

Spatial current distribution in semiconductor optical amplifiers with ridge waveguides and quantum well-dot active region

© A.A. Kharchenko[1], A.M. Nadtochiy[2], G.O. Kornyshov[3], N.Yu. Gordeev[3], A.S. Payusov[3], Yu.M. Shernyakov[3], A.A. Beckman[3], O.I. Simchuk[1], Yu.S. Tkach[1], M.V. Maximov[1]

[1] Alferov Federal State Budgetary Institution of Higher Education and Science Saint Petersburg National Research Academic University of the Russian Academy of Sciences, St. Petersburg, Russia
[2] HSE University, St. Petersburg, Russia
[3] Ioffe Institute, St. Petersburg, Russia

e-mail: antoshkerrr@gmail.com

Received May 06, 2025
Revised June 01, 2025
Accepted October 24, 2025

The spatial distribution of pump current in the active region of a quantum well-dot semiconductor optical amplifier was experimentally determined by identifying boundaries separating gain and absorption zones under varying injection currents and input wavelengths. The spatial non-homogeneity of the pump current distribution for a 5 μm-wide waveguide was found to be less than 14%.

Keywords: quantum well-dots, semiconductor optical amplifiers, transparency current, non-homogeneity of gain,spatial distribution.

DOI: 10.61011/EOS.2025.10.62561.8115-25

Semiconductor optical amplifiers (SOAs) in the 900−1100 nm range are key components of tunable lasers used in spectroscopy and optical coherence tomography — a method for imaging the internal structure of biological objects using light [1]. Heterostructures with InGaAs/GaAs „Quantum well-dot“ (QWD) active regions and GaAs/AlGaAs waveguides have proven effective as prototypes for SOAs in the 1000−1100 nm range [2]. One direction of research and optimization for such devices is achieving spatially uniform gain in the SOA active region [3], since inhomogeneity can degrade the output signal quality. Among the main causes of spatial gain inhomogeneity, one can highlight the high rate of surface charge carrier recombination [4], which leads to reduced population in near-surface regions in devices etched through the active region; the presence of a lateral gradient in pump current density in the active region [5,6]; and the presence of a vertical gradient in charge carrier concentration due to peculiarities of their transport in multilayer active regions [7].

In this work, the spatial distribution of pump current in the SOA active region was experimentally determined by identifying the boundaries between absorption and gain zones at various currents and for various radiation wavelengths. The method is based on the transparency current determination technique proposed in [8].

Fig. 1 shows a simplified experimental schematic. The studied sample is an SOA based on a waveguide $p-i-n$ AlGaAs/GaAs heterostructure grown by metalorganic vapor phase epitaxy on an n^+-GaAs substrate misoriented in the [111] direction by 6°. The active region consists of five different QD layers separated by 40 nm thick GaAs spacers. The QWD layers were formed by deposition of 4, 5, 6, 7, and 9 monolayers of $In_{0.4}Ga_{0.6}As$ and correspond to wavelengths of fundamental optical transitions 985, 1015, 1040, 1060, and 1075 nm. Samples 0.5 mm long with a narrow ridge waveguide of width 5 μm were fabricated from the grown structure. The ridge was formed by plasma-enhanced chemical etching of the p AlGaAs layer to a residual thickness of $\sim$ 300 nm. An electrical contact was formed on the ridge surface.

The sample was placed on a temperature-stabilized copper heat sink at 20 °C, which in turn was mounted on a piezo-platform providing positioning accuracy up to 100 nm in three directions. Intensity-modulated radiation from a tunable Sacher laser (990−1075 nm) was focused onto the sample edge using a micro-objective (×100/NA0.5).

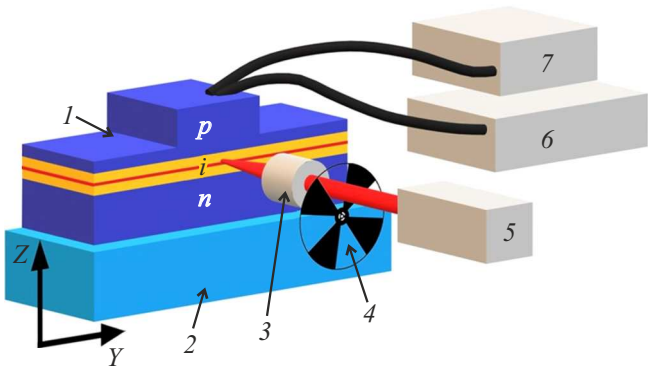

Figure 1. Experimental schematic: *1* — semiconductor optical amplifier including *p*-, *n*-AlGaAs-emitters, *i* — GaAs-waveguide layer containing the active region with QWDs (marked by red line); *2* — piezo-platform; *3* — micro-objective; *4* — modulator; *5* — laser; *6* — lock-in amplifier; *7* — DC power supply.

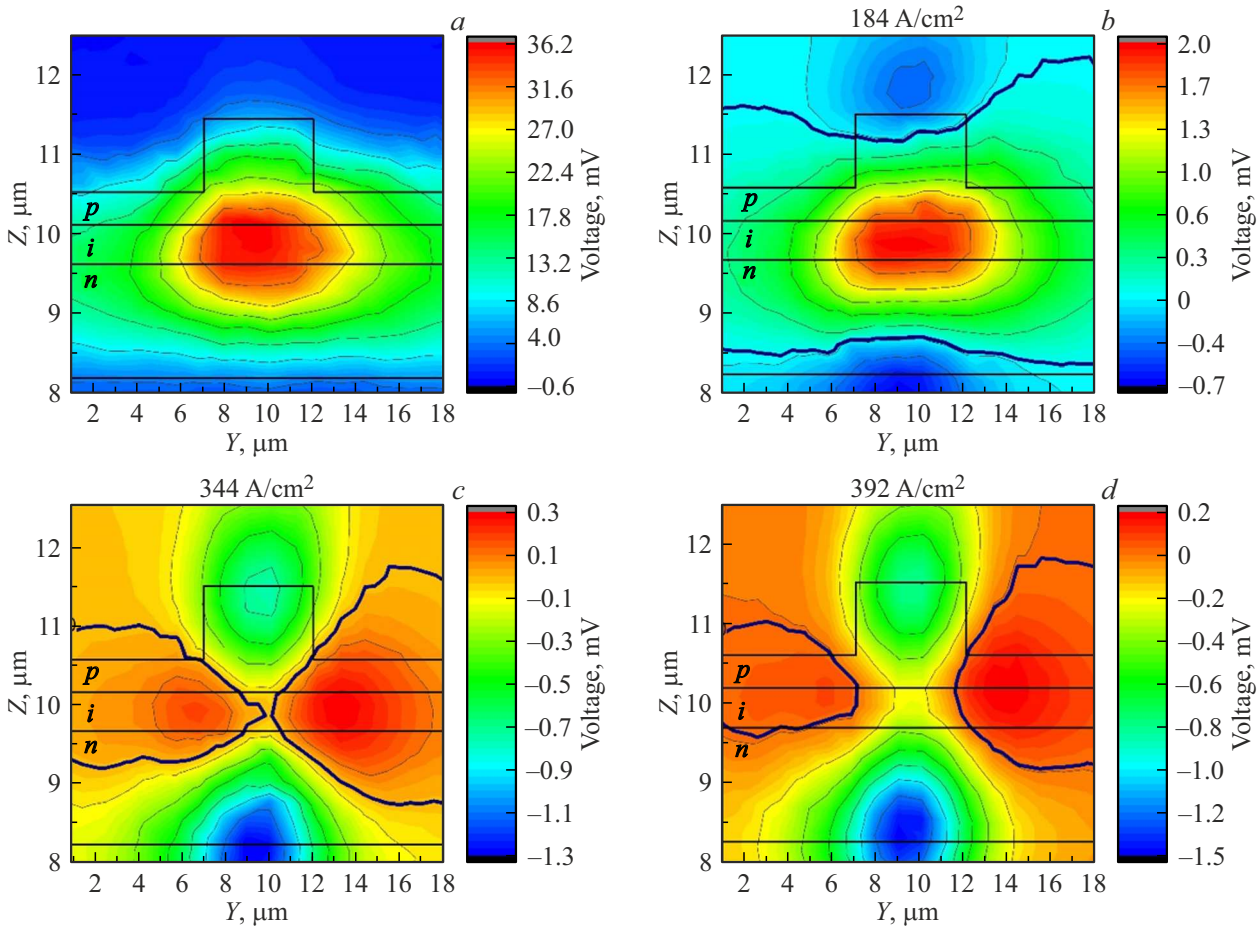

Figure 2. Maps of voltage pulse values versus focused radiation coordinate at wavelength 1040 nm, obtained at pumping currents: 0 (*a*), 4.6 (*b*), 8.6 (*c*), 9.8 mA (*d*). The thickened blue line shows the boundary between regions of positive and negative pulses (gain and absorption). Thin black lines show the sample contours and heterointerfaces. Each figure shows an individual color-to-voltage amplitude correspondence.

Continuous adjustable pumping current was supplied to the sample, and the amplitude of voltage pulses at the radiation modulation frequency was measured. Focusing the Sacher laser radiation at various points on the chip edge (coordinates) leads to preferential excitation of transverse modes that most effectively overlap with the focus region. This enables transverse scanning of the interaction between incoming radiation and the active region inside the waveguide along the y and z coordinates (Fig. 1). Considering the micro-objective characteristics and the tunable laser output beam, the spatial resolution of such scanning was estimated as $1.4\,\mu$m.

Depending on the degree of carrier population, which is determined by the pumping current, three different interaction scenarios are possible between the active region section and the incident radiation: absorption, gain, and transparency mode. Illuminating the sample at low initial non-equilibrium charge carrier concentration leads to radiation absorption in the active region, generation of additional electron-hole pairs, and correspondingly increased carrier population, which in turn causes an increase in sample voltage (optical pumping). At high initial carrier concentration, if the sample is above the transparency threshold for the incident radiation wavelength, the latter increases the rate of stimulated radiative recombination. This leads to a decrease in non-equilibrium carrier concentration and correspondingly a decrease in sample voltage. When using time-modulated radiation, the measured voltage pulses at the optical modulation frequency will have different polarities in the first and second cases. Thus, it is possible to determine whether the illuminated part of the active region is in absorption or gain mode, and to find the pump current value at which modulated illumination does not cause voltage pulses to appear, while the studied local section of the active region is transparent to incident radiation at the given wavelength [2,8].

Fig. 2 shows measurement results as spatial maps of the sample edge, where the color scale indicates the measured voltage pulse amplitude, whose sign corresponds to polarity, and coordinates show the radiation focus location at wavelength 1040 nm. Pumping current values at which the maps were obtained are indicated above. Corresponding

current density values through the stripe p-contact are given in parentheses. In the absence of pump current (Fig. 2, *a*), the registered voltage pulses correspond to the sample's photovoltage. The region of maximum photovoltage is located in the waveguide area under the stripe p-contact. Based on this fact, we were able to map the sample edge contours while maintaining the ridge profile dimensions and thicknesses of p-, i-, n-layers, as shown in Fig. 2, *a*. On the presented maps, non-zero measured pulse values lie within the device boundaries considering the $1.4\,\mu$m resolution.

At pump current increased to 4.6 mA, the voltage pulse amplitude when focusing in the waveguide region under the ridge decreases from 36 to 2 mV (Fig. 2, *b*). Additionally, focusing at the upper boundary of the p-emitter and the lower boundary of the n-emitter leads to negative voltage pulses. We attribute this fact to radiation interaction with charge carriers in heavily doped layers (hot carrier absorption), as a result hot carriers influence the registered voltage pulses up to polarity reversal. However, these phenomena are not related to gain in the active region, so in further analysis we will limit ourselves to examining only the $i$waveguide layer. At current increased to 8.6 mA (Fig. 2, *c*) and focusing in the center of the waveguide layer, the registered voltage pulses change sign to negative. This means that the active region in this spatial part transitions to gain mode. Meanwhile, the lateral parts of the active region remain in absorption mode. We marked the boundary between gain and absorption zones on the maps with thickened blue isolines. With further current increase, the gain zone in the active region smoothly expands laterally and at 9.8 mA (Fig. 2, *d*) already reaches a width of $5\,\mu$m covering the entire waveguide under the ridge.

Spatial maps of voltage pulses were recorded with reduced pump current step over the range corresponding to lateral expansion of the gain zone from the ridge center to its edges, for wavelengths of 1040 nm and 1075 nm. From these data, spatial maps were constructed, showing the position of the boundary between the central gain zone and the side absorption regions at different pump currents (Fig. 3). From these maps, lateral coordinates of boundaries between gain and absorption zones in the i-layer at various pumping currents I for wavelengths 1040 and 1075 nm were determined (Fig. 4, *a*, axis centered at ridge middle). Since these boundaries are in the the transparency regime, it can be stated that the central part of the waveguide under the ridge transitions to transparency regime at lower pump current values (designated as $I_{\min}$) compared to lateral regions, which reach transparency at higher current values. Assuming that the active region is uniform in the $Y-Z$ plane, we consider that transparency regime at its various points will correspond to the same values of local current density J_{tr}. Given that in the considered narrow range of pump currents the active region characteristics change insignificantly (carrier lifetimes, current spreading characteristics, etc.), it can be assumed that the lateral profile of local current density remains unchanged, and an increase in pump current leads to its proportional scaling.

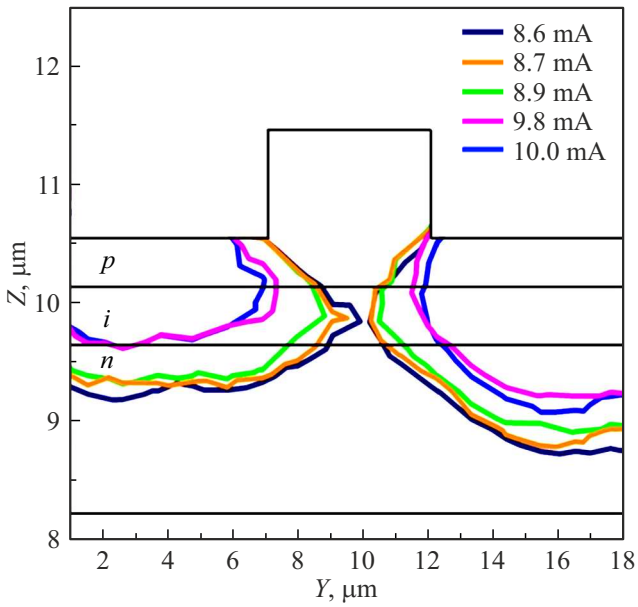

Figure 3. Sample map with the boundary between gain zone (central part) and absorption zone depending on pump current for wavelength 1040 nm. Thin black lines show the sample contours and heterointerfaces.

The above can be expressed as the following proportion:

$$\frac{J(Y)}{J_{tr}} = \frac{I_{\min}}{I}, \qquad (1)$$

where $J(Y)$ — the value of local current density at the point with coordinate Y at current $I_{\min}$. Expression (1) allows calculation of the lateral profile of local current density normalized to its maximum value as $J(Y) = I_{\min}/I$ (Fig. 4, *b*).

Note that the profiles obtained for both wavelengths demonstrate good agreement and edge drop of no more than 14 %. The coincidence of profiles calculated from studies at different wavelengths, and thus at different carrier population levels in the active region, indicates the validity of the assumption about the invariance of the local current density profile shape under the experimental conditions and performed calculations. Since optical amplification in the vicinity of the transparency current is approximately linearly dependent on pumping current in the first approximation [9], the lateral gain profile will have the same shape as the local current density profile, which can lead to optical mode selection in stripe lasers due to spatially inhomogeneous amplification. We also note that the local current density drop at the ridge boundary to 86 % of the maximum indicates that a significant portion of injected carriers recombines outside the ridge waveguide region, which may be important for practical applications of such device designs. For more accurate assessment, a calculation of the current spreading profile and approximation of the obtained data will be performed in the future.

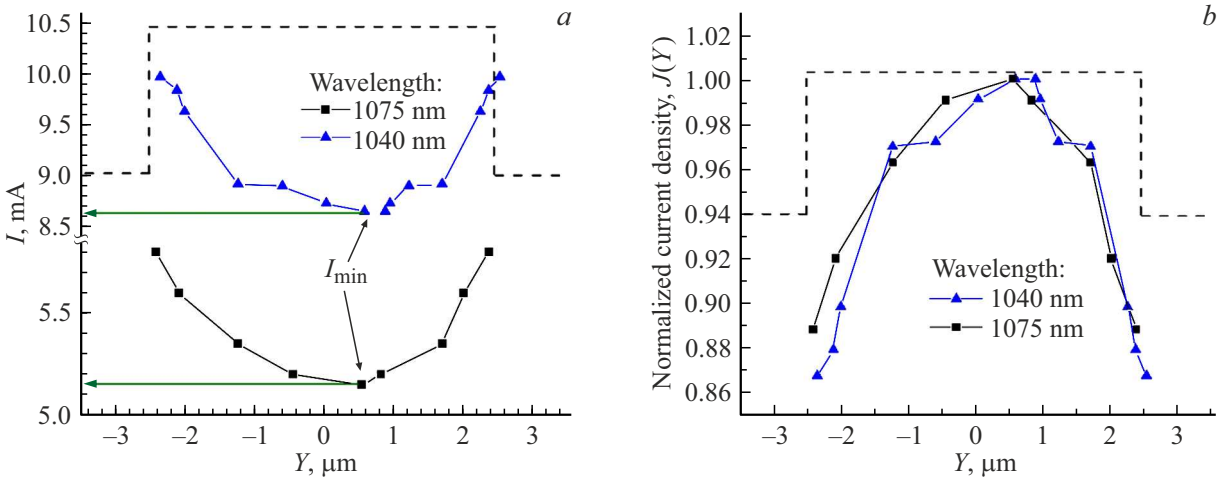

Figure 4. (*a*) Pumping current values at which transparency conditions are achieved in the active region at the corresponding distance from the ridge center (Y) for radiation wavelengths 1040 (blue lines) and 1075 nm (black lines); (*b*) normalized profiles of local current density. Dashed lines show the ridge profile.

Thus, a method has been proposed for determining the lateral current distribution profile in ridge emitting structures. In the transverse plane of a sample with a ridge waveguide, boundaries separating active region zones in gain regime from those in absorption regime were found at various pump currents and radiation wavelengths. The obtained results enabled calculation of the lateral local current density profile and assessment of the spatial position of the optical amplification zone depending on pumping current in an SOA with a wavelength-chirped QWD active region. The spatial inhomogeneity of pumping current distribution within the 5 μm-wide ridge was less than 14 %.

Acknowledgments

O.I. Simchuk wishes to thank the Ministry of Science and Higher Education of the Russian Federation (project FSRM-2023-0010) for supporting the study of chip edge morphology by atomic force microscopy. A.M. Nadtochiy wishes to thank the HSE University Fundamental Research Program for supporting the work on mathematical processing of two-dimensional experimental data maps

Funding

This study was supported by the Russian Science Foundation, grant № 23-72-00038, https://rscf.ru/project/23-72-00038/.

Conflict of interest

The authors declare that they have no conflict of interest.

References

[1] A.A. Lobintsov, M.V. Shramenko, S.D. Yakubovich. Kvant. elektron., **38**, 661 (2008) (in Russian).

[2] A.A. Harchenko, A.M. Nadtochij, Yu.M. Shernyakov, N.Yu. Gordeev, A.S. Payusov, A.A. Bekman, G.O. Kornyshov, O.I. Simchuk, Yu.A. Salij, M.M. Kulagina, N.A. Mintairov, S.A. Kalyuzhnyj, M.V. Maksimov. FTP **58**, 313 (2024) (in Russian).

[3] D. Ban, E.H. Sargent. IEEE J. Quant. Electron., **36**, 1081 (2000).

[4] C. Cruz, C. Caló, F. Pommereau, A. Wilk, O. Delorme, N. Vaissiére, J. Decobert, H. Carrere. In: *2024 24th Int. Conf. Transparent Opt. Networks* (IEEE, 2024), p. 1–5.

[5] J. Fricke, H. Wenzel, A. Maaßdorf, C. Zink, M. Matalla, R. Unger, A. Knigge. Semicond. Sci. Technol., **37**, 095021 (2022).

[6] A.S. Payusov, M.I. Mitrofanov, G.O. Kornyshov, A.A. Serin, G.V. Voznyuk, M.M. Kulagina, V.P. Evtikhiev, N.Yu. Gordeev, M.V. Maksimov, S. Breuer. Pisma v ZhTF **47**, 51 (2021) (in Russian).

[7] M. Rossetti, P. Bardella, M. Gioannini, I. Montrosset. *Proc. 14th Eur. Conf. Integr. Opt. Tech. Exhib. Contrib. Invit.* (2008), p. 221.

[8] P.A. Andrekson, N.A. Olsson, T. Tanbun-Ek, R.A. Logan, D. Coblentz, H. Temkin. Electron. Lett., **28**, 171 (1992).

[9] L.A. Coldren, S.W. Corzine, M.L. Mashanovitch. *Diode Lasers and Photonic Integrated Circuits* (Wiley, 2012).

Translated by J.Savelyeva